STEM CELLS®

TRANSLATIONAL AND CLINICAL RESEARCH

Intratumoral Delivery of Interferonγ-Secreting Mesenchymal Stromal Cells Repolarizes Tumor-Associated Macrophages and Suppresses Neuroblastoma Proliferation In Vivo

THERESA RELATION [a,b], TAI YI,[c] ADAM J. GUESS,[b] KRISTA LA PERLE,[d] SATORU OTSURU,[b] SUHEYLA HASGUR,[b] MASSIMO DOMINICI,[e] CHRISTOPHER BREUER,[c] EDWIN M. HORWITZ[b]

Key Words. Mesenchymal stem cells • Microenvironment • Immunotherapy • Cancer • Cellular therapy

[a]The Ohio State University Medical Scientist Training Program, Columbus, Ohio, USA; [b]Center for Childhood Cancer and Blood Diseases; [c]Center for Cardiovascular Research, The Research Institute at Nationwide Children's Hospital, Columbus, Ohio, USA; [d]Department of Veterinary Biosciences, The Ohio State University, Columbus, Ohio, USA; [e]Department of Medical and Surgical Sciences of Children and Adults, University of Modena and Reggio Emilia, Modena, Italy

Correspondence: Edwin M. Horwitz, M.D., Ph.D., Aflac Cancer and Blood Disorders Center, Children's Healthcare of Atlanta, Emory University Department of Pediatrics, 2015 Uppergate Drive, Atlanta, Georgia 30322-1015, USA. Telephone: 404-727-1958; e-mail: edwin.horwitz@emory.edu

Received November 2, 2017; accepted for publication January 31, 2018; first published online in STEM CELLS *EXPRESS* February 12, 2018.

http://dx.doi.org/10.1002/stem.2801

ABSTRACT

Neuroblastoma, the most common extracranial solid tumor in childhood, remains a therapeutic challenge. However, one promising patient treatment strategy is the delivery of anti-tumor therapeutic agents via mesenchymal stromal cell (MSC) therapy. MSCs have been safely used to treat genetic bone diseases such as osteogenesis imperfecta, cardiovascular diseases, autoimmune diseases, and cancer. The pro-inflammatory cytokine interferon-gamma (IFNγ) has been shown to decrease tumor proliferation by altering the tumor microenvironment (TME). Despite this, clinical trials of systemic IFNγ therapy have failed due to the high blood concentration required and associated systemic toxicities. Here, we developed an intra-adrenal model of neuroblastoma, characterized by liver and lung metastases. We then engineered MSCs to deliver IFNγ directly to the TME. In vitro, these MSCs polarized murine macrophages to the M1 phenotype. In vivo, we attained a therapeutically active TME concentration of IFNγ without increased systemic concentration or toxicity. The TME-specific IFNγ reduced tumor growth rate and increased survival in two models of T cell deficient athymic nude mice. Absence of this benefit in NOD SCID gamma (NSG) immunodeficient mouse model indicates a mechanism dependent on the innate immune system. IL-17 and IL-23p19, both uniquely M1 polarization markers, transiently increased in the tumor interstitial fluid. Finally, the MSC vehicle did not promote tumor growth. These findings reveal that MSCs can deliver effective cytokine therapy directly to the tumor while avoiding systemic toxicity. This method transiently induces inflammatory M1 macrophage polarization, which reduces tumor burden in our novel neuroblastoma murine model. STEM CELLS *2018; 00:000–000*

SIGNIFICANCE STATEMENT

Despite the rapidly expanding field of immune therapy, major advances in the treatment of solid tumors have not been realized. This is due in part to the protective tumor microenvironment, which fashions an immune suppressive milieu that hinders immune responses. This article demonstrates proof-of-concept that directly introducing interferon-γ secreting mesenchymal stromal cells (MSCs) into an orthotopic neuroblastoma xenograft can induce transient macrophage repolarization and a pro-inflammatory environment without systemic cytokine exposure. While MSC-delivered interferon-γ showed anti-tumor activity alone, further tangible benefits may lie in potentiating existing and future therapies to develop effective solid tumor cellular immune therapy.

INTRODUCTION

Neuroblastoma is the most common extracranial solid tumor in childhood and arises from the developing nervous system's sympathetic ganglia [1]. Tumors commonly occur in the adrenal gland or in the paraspinal sympathetic chain; specific genetic mutations of the tumor, age at diagnosis, and local invasiveness/metastasis are used to stratify patients into risk groups for treatment. The most common genetic mutation in neuroblastoma occurs in the *MYCN* gene, with gene amplification (>10 copies) being one of the most important prognostic indicators. The standard of care consisting of surgical resection, chemotherapy, and radiotherapy has not changed for decades. While many low-risk patients will

achieve long-term survival, high-risk patients will frequently relapse with aggressive, therapy-resistant tumors [2]. Currently we lack established, effective therapies for these patients. Thus, those that do not respond to the primary therapy are left in the unacceptable position of having a dismal prognosis without standard treatment options.

The only optimistic exception to this state is the development of dinutuximab, a monoclonal antibody directed at GD2 expression on neuroblastoma cells, which fosters immune-mediated tumor elimination [3]. Dinutuximab's FDA approval in 2015 signified acceptance of the idea that immune therapy can be used to treat neuroblastoma. However, the insufficient response to new cellular therapies (e.g., chimeric antigen receptor-expressing T cells) reminds us that the immune-suppressive tumor microenvironment (TME) remains a major obstacle to increasing the long-term survival of children with neuroblastoma.

Effectively killing cancer cells is complicated by multiple factors within the TME [4]. For example, cancer cells secrete a dense matrix which physically impedes the body's immune cells or drugs from accessing the cancer cells. Moreover, drug and immune cell penetration is impaired by convoluted, disorganized vasculature. Nonetheless, immune cells such as tumor infiltrating lymphocytes (TILs) and tumor-associated macrophages (TAMs) do find their way into the tumor but are either ineffective due to the immune suppressive microenvironment (e.g., TILs) or worse, contribute to immune suppression themselves (e.g., TAMs). This latter mechanism is particularly important because immunity should be the body's best defense against cancer. By abrogating immune suppression in the TME and stimulating the immune cells to regain responsiveness, it may be possible to reactivate immune defense against cancer.

In this work, we use mesenchymal stromal cells (MSCs) as vehicles to deliver the pro-inflammatory cytokine interferon-gamma (IFNγ). MSCs are found throughout the body but migrate to specific tissues in the context of remodeling and regeneration [5]. In some cancers, MSCs can suppress antitumor immune activity in the tumor tissue [6]. However, MSCs are a valuable treatment tool because they can be readily modified to robustly secrete immune-modulating molecules [7, 8]. Our group was the first to infuse allogeneic MSCs into pediatric patients with osteogenesis imperfecta and the first to introduce genetically modified MSCs into patients [9]. There are over 950 MSC clinical trials in place, as of January 2018, focusing on all organ systems (https://ClinicalTrials.gov).

Here, we exploit the treatment potential of MSCs by engineering human MSCs to express and secrete IFNγ, one of the most important molecules in suppressing cancer development and progression [10]. IFNγ has been shown to decrease blood vessel formation in tumors, increase immune cell activation and the consequent recognition of cancer cells, and decrease cancer cell proliferation [11]. IFNγ has been approved for the treatment of adult T cell leukemia in Japan, but clinical trials in the United States, while promising, have yet to yield an FDA-approved cancer treatment [12]. Despite the positive effects of IFNγ on cancer cells, systemic administration is associated with significant adverse side effects, including nausea, depression, fever, and leukopenia [13]. By directly introducing IFNγ into the tumor, we propose to eliminate systemic toxicities while preserving the anti-cancer benefits. Here, we demonstrate that direct injection of IFNγ-expressing MSCs into the tumor activates the innate immune system, resulting in decreased tumor growth and increased overall survival.

Materials and Methods

Lentivirus Generation and Transfection

Lentiviruses were generated in HEK293T/17 cells using pHIV-enhanced green fluorescent protein (EGFP), a gift from Bryan Welm & Zena Werb (Addgene 21373, Cambridge, USA), psPAX2, a gift from Didier Trono (Addgene plasmid # 12260), and pMD2.G, a gift from Didier Trono (Addgene plasmid # 12259). Human *IFNγ* (gene ID 3458) and murine *IFNγ* (gene ID 15978) were cloned into the plasmid at the BamHI insertion site. Lentiviral titers were determined as described in [14].

MSCs

MSCs were isolated and expanded as previously described [15]. The marrow was taken from the residua (waste) of bone marrow harvest collection bags obtained from healthy donors undergoing marrow harvest for clinical indications. The protocol was classified as exempt from oversight by the Institutional Review Board of Nationwide Children's Hospital. At passage 3, we confirmed that these MSCs met the criteria proposed by International Society for Cellular Therapy [16].

Cell Culture

CHLA-255 cells expressing luciferase (CHLA-255-luc) and CHLA-20 neuroblastoma cell lines were generously provided by Dr. Shahab Asgharzadeh at the Children's Hospital of Los Angeles. CHLA-255-luc and CHLA-20 cells were grown in IMDM modified media (Iscove's Modified Dulbecco's Medium) (GE Healthcare, Chicago, USA) supplemented with 1% antibiotic solution (Corning, New York, USA) and 20% fetal bovine serum (FBS) (Gemini Bio-Products, Sacramento, USA). Primary murine macrophages were cultured in Dulbecco's modified Eagle's medium (Corning Cellgro) supplemented with 1% antibiotic/antimycotic solution and 10% FBS and 30% L929-cell conditioned medium as a source of granulocyte/macrophage colony stimulating factor [17]. Recombinant murine IFNγ (mIFNγ) was obtained from PeproTech (Rocky Hill, USA). Cell proliferation was measured using colorimetric MTS assay (BioVision, San Francisco, USA).

Primary Murine Macrophages

Femurs and tibias were obtained from 6–12 week-old C57BL/6 mice. After removal of both epiphyses, a syringe was used to flush phosphate buffered saline (PBS) through the bone marrow cavity to exude bone marrow. Bone marrow homogenates were treated with ammonium-Chloride-Potassium (ACK) lysing buffer to remove red blood cells and placed into culture. Cells were seeded in non-tissue culture treated Petri dishes and cultured for 7 days prior to stimulation. The resulting macrophages were then treated with mIL-4 (30 ng/ml), mIFNγ (50 ng/ml), or co-cultured with equivalent number of MSCs for 4 days.

Mice

NOD SCID gamma mice (NSG, NOD.Cg-*Prkdc*^{scid} *Il2rg*^{tm1Wjl}/SzJ) were obtained from The Jackson Laboratories (Bar Harbor, USA). Colonies of this strain were established and maintained in the vivarium in The Research Institute at Nationwide Children's Hospital. Athymic nu/nu (nude) mice were obtained

from Envigo (Huntingdon, UK). Clinical and anatomic pathology was performed as described in [18]. All animal protocols were approved by the Institutional Animal Care and Use Committees of the Research Institute at Nationwide Children's Hospital.

Establishment of Orthotopic Tumor Model

Female nude mice, aged 6–8 weeks, and female NSG mice, aged 2–4 months, were anesthetized with an i.p. injection of ketamine (100 mg/kg) and xylazine (10 mg/kg). A transverse incision approximately 8 mm in length was made over the left flank just posterior to the spleen and ribcage. Following the opening of skin and underlying muscle, 3.75×10^6 neuroblastoma cells in 100 μl 25% Matrigel (Corning) PBS solution were injected under the adrenal capsule toward the superior pole of the kidney. Muscle and skin were then closed with a 4-0 polysorb suture.

Ultrasound-guidance injection was used to deliver MSCs directly to the tumor when the tumor reached 0.5–1 volume equivalents of the kidney. Injections were done under general anesthesia using isoflurane. Tumor development was monitored via ultrasound (VisualSonics Vevo 770) and bioluminescence. Mice were injected with 30 mg/ml D-luciferin (Biosynth Chemistry and Biology, Staad, Switzerland) 20 minutes prior to imaging using Xenogen IVIS Spectrum. Mice were euthanized upon meeting the following endpoint criteria: any tumor diameter $\geq$1 cm or any animal that demonstrated $>$20% weight loss. Mice were euthanized by terminal cardiac bleed under isoflurane followed by cervical dislocation and vital organ removal. This timing is subsequently denoted "endpoint."

Macrophage Depletion In Vivo

Mice were treated with 200 μl liposomal clodronate or control liposomes (Clodrosome, Brentwood, USA) i.p. 2 days prior to tumor implantation. After tumor implantation, all mice received 100 μl i.p. three times weekly for the duration of the experiment.

Flow Cytometry

All flow cytometry was performed using BD LSR II. Whole tumors were homogenized in PBS solution containing 150 μg/ml DNase 1 (Sigma-Aldrich, St. Louis, USA) and 25 μg/ml liberase blendzyme (Sigma-Aldrich). Tumors were then strained through a 70 μm filter and red blood cells were lysed using ACK lysing buffer (ThermoFisher, Waltham, USA). Tumor cell suspensions were then washed with PBS and stained using the following antibodies: CD45 (BioLegend 103126, San Diego, USA), CD11b (BD Pharmingen 557397, San Jose, USA), F4/80 (BioLegend 123116), and CD90 (Biolegend 328122).

Gene Profiling

RNA was harvested from cells using RNeasy mini kit (Qiagen). cDNA was generated using high-capacity cDNA reverse transcription kit (ThermoFisher). qPCR analysis (quantitative polymerase chain reaction) was performed using Taqman gene expression assays and Applied Biosystems StepOne Plus thermocycler.

Cytokine Profiling

Tumor interstitial fluid (TIF) was collected as described by Haslene-Hox et al. [19]. Briefly, tumors were halved, placed over a 40 μm strainer, and centrifuged at 106*g* for 10 minutes. Blood was collected from mice by terminal cardiac bleed and whole mouse blood was allowed to clot at room temperature for 30 minutes. Serum was isolated from the clots by centrifugation at 1,500*g* for 10 minutes. Cytokine concentration was determined using Bio-Plex kits (Bio-Rad M60009RDPD, 171GA005M, 171V4001M) and Bio-Plex suspension array system.

IFNγ Release and Activity

MSC-mIFNγ cells were cultured for 1–3 days, followed by supernatant collection. Supernatants were clarified by centrifugation at 400*g* for 5 minutes. mIFNγ concentration was determined by ELISA (R&D DY485, Minneapolis, USA). IFNγ activity was determined by cytopathic effect (CPE)-based anti-viral assay (AVA) testing, performed by UCyTech (Utrecht, Netherlands).

Immunofluorescence Staining

Mice were euthanized according to approved protocol and tissue samples were excised. Lungs were partially infused with 10% formalin to expand tissue. Tissue samples were fixed in 10% buffered formalin and embedded in paraffin. Five micrometer sections were mounted to slides. Slides were immersed in 100 nM sodium citrate buffer and placed in decloaking chamber (BioCare Medical, California, USA) for 25 minutes. The following reagents were used: normal donkey serum (Jackson Immunoresearch 017-000-121, West Grove, USA), monoclonal rabbit anti-human CD90 antibody (1:200, Clone EPR3132; Abcam, Cambridge, USA), biotinylated anti-GFP (1:200, Novus Biologicals NB100–1678, St. Louis, USA), DAPI (Life Technologies D3571, Carlsbad, USA), anti-goat Alexa 488 (Invitrogen A11055, Waltham, USA), anti-rabbit Alexa 555 (Invitrogen A31572), ProLong Gold antifade reagent (Invitrogen P36930). Images were taken using Zeiss Axio Imager.A1 and AxioCam MRm Rev.3 at $\times$200 magnification.

Statistical Analysis

Statistical analyses were performed by unpaired two-tailed *t* test for comparison of two samples, and by one-way analysis of variance for multiple samples followed by Tukey's multiple comparisons test, using Prism (Version 6; GraphPad Software, Inc., San Diego, USA). Survival curves were compared using the log-rank Mantel-Cox test. Outliers were identified and removed by extreme studentized deviate method. All data are shown as mean $\pm$ SE. A p value $<$.05 was considered statistically significant. In all figures, statistical significance is indicated as follows: (*) denotes $p < .05$, (**) denotes $p \leq .01$, (***) denotes $p \leq .001$, (****) denotes $p \leq .0001$, and (n.s.) or no symbol represents no significant difference.

Results

Intra-Adrenal Neuroblastoma Xenograft Model

In an effort to study the clinically relevant role of the TME in neuroblastoma, we developed an intra-adrenal xenograft model of human neuroblastoma. We chose to use nude mice, which lack

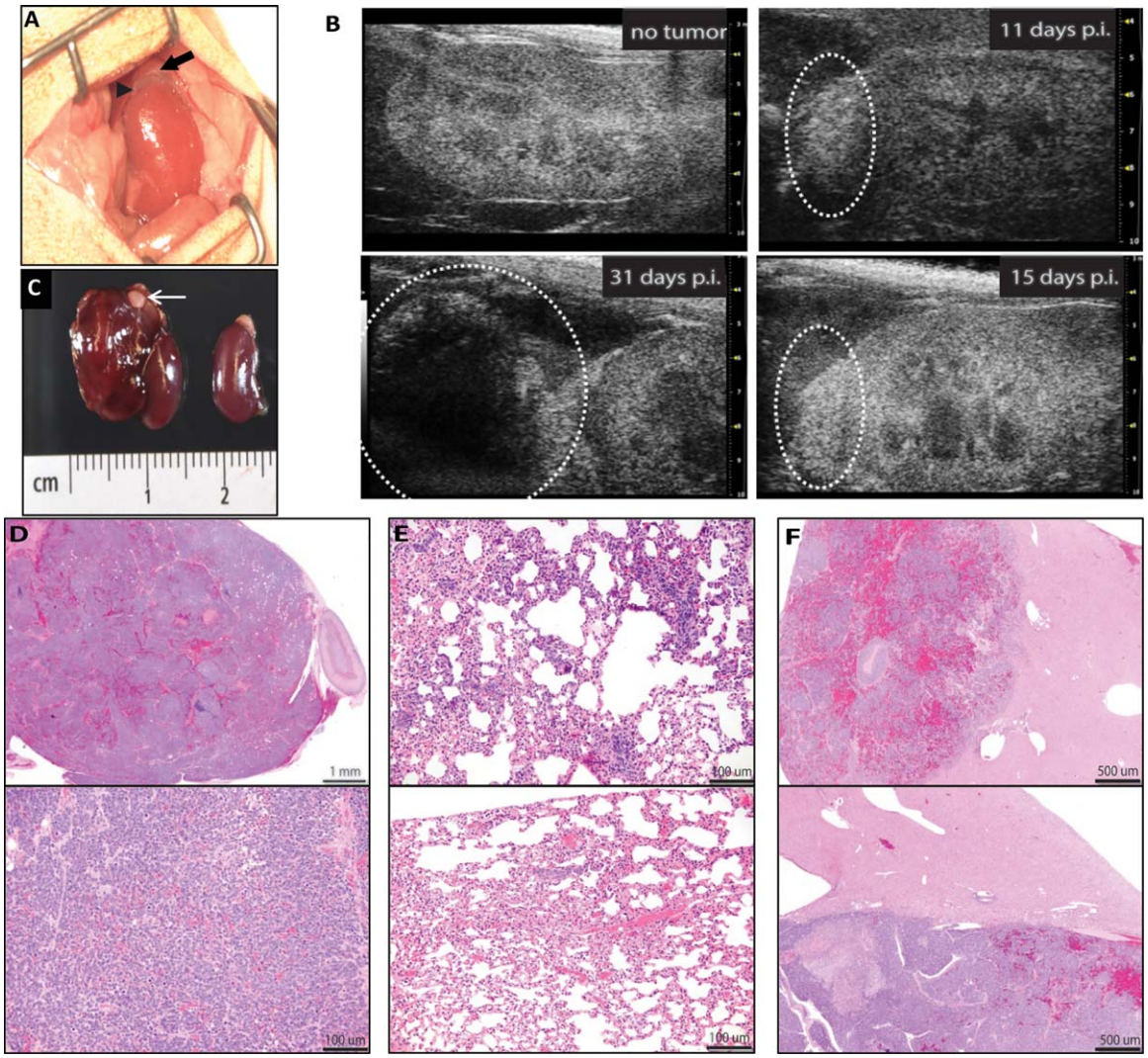

Figure 1. Intra-adrenal capsule murine model of neuroblastoma. CHLA-255-luc or CHLA-20 human neuroblastoma cells suspended in 25% Matrigel (arrowhead) were injected into the adrenal capsule caudal to the adrenal gland (solid arrow) **(A)**. Tumors were identifiable via ultrasound between 10 and 14 days post-injection (p.i.). Clockwise from top left: no tumor, 11, 15, 31 days p.i. Tumors are circled by white dotted line **(B)**. Tumors spared ipsilateral kidney and adrenal gland (white arrow) on gross histology **(C)**. Representative H&E staining of tumor **(D)**, lung metastases **(E)**, and liver metastases **(F)**.

functional T cells, in order to explore the role of the innate immune system in the absence of T cell immunity. CHLA-255 cell line, derived from human neuroblastoma metastatic site, was chosen due to its reported high CCL2 expression levels and sensitivity to macrophage polarization [20]. After CHLA-255-luc cells were injected under the adrenal capsule (Fig. 1A), tumors could be first visualized via ultrasound at 10–14 days as indicated by an opaque structure anterior to the kidney (identified by visible renal pyramids) (Fig. 1B). Tumors became palpable through the skin near endpoint, and calipers were used to determine endpoint for mice based on a tumor diameter $\geq$1 cm.

Gross analysis of the tumors revealed minimal invasion into the ipsilateral kidney. Ipsilateral adrenal glands were spared by the tumor, and contralateral kidneys demonstrated no gross abnormalities (Fig. 1C). Histological analyses of the tumors were consistent with neuroblastoma, with dense hypercellularity [21] (Fig. 1D). Metastases were identified in lungs and liver (Fig. 1E, 1F), consistent with sites of metastasis found clinically [2, 22].

Generation of mIFNγ-Expressing MSCs

Human MSCs were transduced with a bicistronic lentiviral vector that expresses mIFNγ and EGFP under the control of the viral long terminal repeat (LTR). Transduction efficiency at day 3 was 89.7% $\pm$ 0.8%, $n = 3$ (Fig. 2A). Transduced MSCs secreted 69.1 $\pm$ 14.3 pg mIFNγ/10^6 MSCs/24 hours (Fig. 2B) and exhibited no difference in proliferation over 5 days (Supporting Information Fig. S1). To confirm the biologic activity of mIFNγ secreted from human MSCs, we compared our secreted cytokine with commercially available recombinant mIFNγ. MSC-secreted mIFNγ showed 1.2 $\pm$ 0.25 $\times$ 10^7 units/mg protein which was statistically similar to the activity of recombinant mIFNγ (4.9 $\pm$ 0.1 $\times$ 10^6 units/mg protein) assayed in parallel (Fig. 2C). IFNγ activity was determined by CPE-based AVA testing, performed by UCyTech.

MSC-mIFNγ Induces M1 Macrophage Polarization In Vitro

We next examined the ability of mIFNγ-secreting MSCs (MSC-mIFNγ) to polarize primary murine macrophages in vitro.

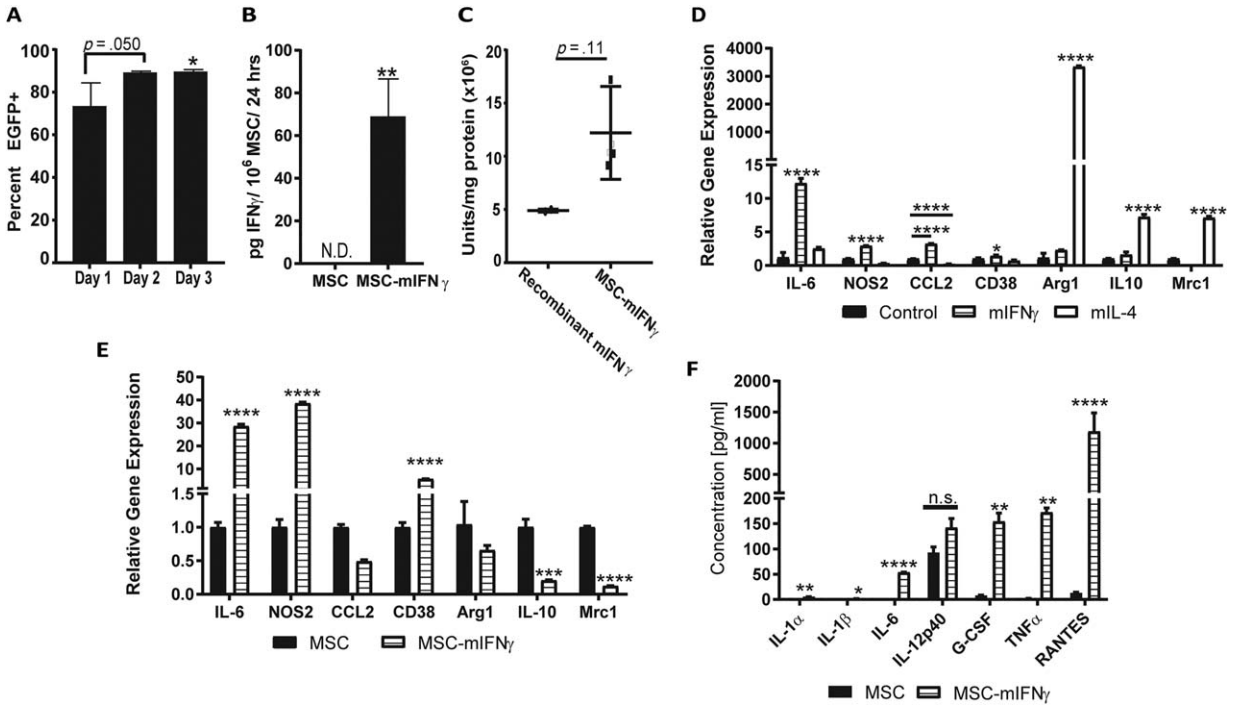

Figure 2. MSC-mIFNγ polarize M1 macrophages in vitro. Bicistronic lentiviral vector that expresses murine interferon-gamma (mIFNγ) and EGFP reaches peak infectivity 3 days post-infection in human MSCs ($p = .0455$) **(A)**. MSC-mIFNγ release 69.1 ± 14.3 pg mIFNγ/10^6 MSCs/24 hours ($p = .0024$) **(B)**. Activity of lentivirally-produced mIFNγ was not statistically different when compared to recombinant mIFNγ **(C)**. Bone marrow-derived macrophages (BMDM) cultured with 30 ng/ml recombinant mIL-4 demonstrated increased mRNA expression of M2 activation markers Arg1, IL-10, and Mrc1 **(D)**. BMDM cultured with recombinant mIFNγ 50 ng/ml (D) and BMDM co-cultured with MSC-mIFNγ **(E)** demonstrated increased mRNA expression of M1 activation markers IL-6, NOS2, and CD38, while CCL2 was upregulated in recombinant mIFNγ treated BMDM only. Co-culture of MSC-mIFNγ with BMDM increases cytokine expression of IL-1α ($p = .0023$), IL-1β ($p = .0231$), IL-6 ($p < .0001$), G-CSF ($p = .0064$), TNFα ($p = .0012$), and RANTES ($p = 0.0308$). IL-12p40 was not significantly upregulated **(F)**. Statistical significance is indicated as follows: (*) denotes $p < .05$, (**) denotes $p \leq .01$, (***) denotes $p \leq .001$, (****) denotes $p \leq .0001$, and (n.s.) or no symbol represents no significant difference. Abbreviations: EGFP, enhanced green fluorescent protein; mIFNγ, murine interferon-gamma; MSC, mesenchymal stromal cell; N.D., not detected.

Primary bone marrow-derived macrophages (BMDM) were treated with 50 ng/ml recombinant mIFNγ (M1) or 30 ng/ml recombinant mIL-4 (M2) for 4 days. Following cell harvest and cDNA synthesis, samples were probed for expression of M1 polarization markers IL-6, NOS2, CCL2, and CD38 [23–25] and M2 polarization markers Arg1, IL-10, and Mrc1/CD206 [26, 27]. Compared to untreated cells, BMDM exposed to mIFNγ demonstrated significantly increased expression of M1 markers while BMDM exposed to mIL-4 demonstrated significantly increased expression of M2 markers (Fig. 2D). This process was then repeated using BMDM co-cultured with MSC-mIFNγ and control MSCs. Co-culture of BMDM with MSC-mIFNγ similarly significantly increased expression of these M1 markers and decreased expression of M2 markers (Fig. 2E). Fold changes for each gene are listed in Table 1.

Supernatants from co-culture samples were analyzed for cytokine expression. Co-culture with MSC-mIFNγ increased expression of inflammatory M1-related cytokines IL-1α, IL-1β, IL-6, G-CSF, TNFα, and RANTES/CCL5, but no significant change in IL-12p40 (Fig. 2F). These findings indicate that MSC-mIFNγ polarize macrophages to the inflammatory M1 phenotype in vitro. Despite reports that unmodified MSCs can polarize macrophages toward the M2 alternative activation phenotype [28, 29], our findings suggest that the presence of MSCs does not impede the polarizing effect of mIFNγ.

Table 1. Gene expression changes in primary bone marrow-derived macrophages in vitro

	mIFNγ vs. control		mIL-4 vs. control		MSC-mIFNγ vs. MSC	
Gene	Fold change	*p* value	Fold change	*p* value	Fold change	*p* value
IL-6	12.3 ± 4.7	.0001	2.5 ± 0.2	.0578	28.6 ± 0.7	<.0001
NOS2	2.9 ± 0.2	.0001	0.3 ± 0	.0001	38.5 ± 0.5	<.0001
CCL2	3.2 ± 0.9	.0001	0.2 ± 0	.0001	0.5 ± 0	.3800
CD38	1.4 ± 0.4	.0174	0.7 ± 0.1	.0519	5.6 ± 0.1	<.0001
Arg1	2.3 ± 0.4	.9956	3,342.9 ± 21.4	.0001	0.7 ± 0.1	.1332
IL-10	1.6 ± 0.8	.0069	7.3 ± 0.3	.0001	0.2 ± 0	.0003
Mrc1	0.2 ± 0	.0004	7.1 ± 0.2	.0001	0.1 ± 0	<.0001

BMDM were cultured in mIFNγ or mIL-4, and gene expression changes were compared to untreated BMDM. BMDM were co-cultured with MSC-mIFNγ, and gene expression changes were compared to co-culture with MSC.
Abbreviations: BMDM, bone marrow-derived macrophages; mIFNγ, murine interferon-gamma; MSC, mesenchymal stromal cell.

MSC-mIFNγ Slows Tumor Growth and Increases Overall Survival

Next, we examined the effect of MSC-mIFNγ delivered directly into the TME. Because IFNγ does not cross-react between mouse and human, mIFNγ introduced into the tumor will stimulate murine cells only, including the immune system, but will not directly affect the human tumor nor have an autocrine effect on the human MSCs. Ultrasound tumor monitoring revealed the average time for the tumors to reach

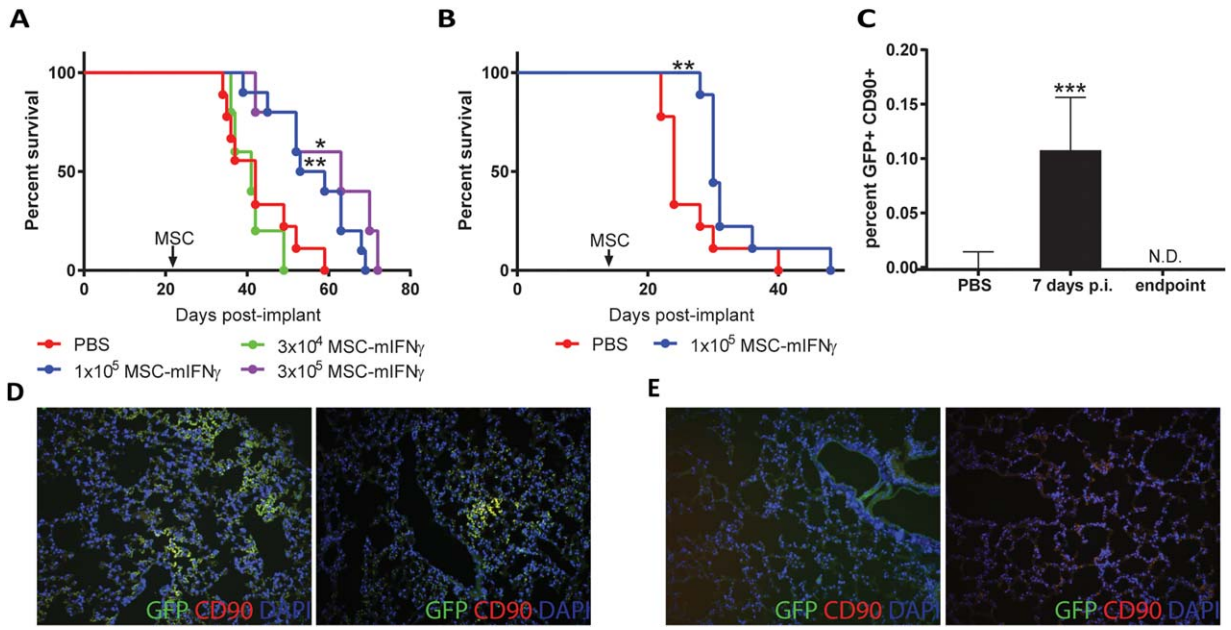

Figure 3. MSC-mIFNγ increases survival in intra-adrenal neuroblastoma. CHLA-255-luc tumor-bearing mice were treated with either PBS ($n = 9$), 3×10^4 ($n = 5$), 1×10^5 ($n = 10$), or 3×10^5 MSC-mIFNγ ($n = 5$). 1×10^5 MSC-mIFNγ $p = .0048$, 3×10^5 MSC-mIFNγ $p = .0135$ **(A)**. The minimal effective dose was repeated in CHLA-20 tumor bearing mice ($p = .0066$) **(B)**. GFP+ CD90+ MSC-mIFNγ were identified by flow cytometry in the tumor at 7 days p.i., but were undetectable at endpoint ($p = .0007$) **(C)**. Mice were injected with MSC-mIFNγ intravenously 2 hours prior to lung tissue harvest **(D)**, and lungs from tumor-bearing mice were collected at endpoint **(E)**. Immunofluorescence staining for GFP and human-CD90 revealed MSCs present in the lungs of mice injected with i.v. MSC-mIFNγ but absent in experimentally treated mice at endpoint (representative images shown, ×200 magnification). Abbreviations: GFP, green fluorescent protein; mIFNγ, murine interferon-gamma; MSC, mesenchymal stromal cell; PBS, phosphate buffered saline; p.i., post-injection.

0.5–1 kidney volume equivalents was 21 days after tumor placement. At that time, tumors were directly injected with graded doses of MSC-mIFNγ or PBS. While a dose of 3×10^4 MSC-mIFNγ showed no benefit, doses of 1×10^5 and 3×10^5 MSC-mIFNγ significantly increased overall survival by ≥33% (Fig. 3A). Since the two higher doses did not produce statistically different survival outcomes, we chose to proceed with the minimal effective dose (MED) of 1×10^5 MSC-mIFNγ. Mice treated with MSC-mIFNγ were analyzed at endpoint by postmortem examination to identify occult organ toxicity or tumor formation. The complete blood counts and white blood cell subset proportions were within the expected range for nude mice. Similarly, serum chemistries in the 1×10^5 MSC-mIFNγ treatment group were within the normal range for all mice (data not shown). Metastases were identified in the lungs and liver in all groups, as expected in this neuroblastoma model. We did not identify any additional metastases, non-neuroblastoma occult malignancies, or organ toxicity.

To confirm that this survival benefit is not unique to the CHLA-255-luc tumor model, we next examined MSC-mIFNγ treatment in CHLA-20 human neuroblastoma cell line, derived from primary tumor. This model was chosen because, like CHLA-255, the cell line secretes the macrophage-attracting chemokine CCL2 [20, 30], forming tumors with a relatively abundant population of macrophages. Tumors in this model reached treatment size at 14 days post-implant. In this model, MSC-mIFNγ treatment produced increased survival by 25% compared to controls, similar to the former neuroblastoma model (Fig. 3B).

Because any treatment benefit is constrained by MSC persistence within the tumor, we analyzed MSC content in tumors by flow cytometry. CHLA-255-luc tumors were harvested at 7 days post MSC-mIFNγ injection and at endpoint. While tumors at endpoint did not reveal a measurable population of MSC-mIFNγ, GFP+ human-CD90+ MSCs could be identified in tumors harvested 7 days post-injection (Fig. 3C). Because intravenously injected MSCs may accumulate in the lungs before being cleared through the circulation [31], we next evaluated the lungs of MSC-mIFNγ treated mice. Compared to control mice injected with MSC i.v. 2 hours prior to tissue harvest (Fig. 3D), tumor-bearing mice showed no identifiable GFP+ human-CD90+ MSCs in the lungs (Fig. 3E). These data indicate limited persistence of MSC-mIFNγ within the tumor after a single dose, which may underlie the limited duration of tumor growth suppression.

MSC Delivery Vehicle Does Not Impede IFNγ-Induced Tumor Suppression

The role of MSCs in immune activation remains controversial. MSCs have been characterized as pro-inflammatory in many studies, but other studies reveal an immune-suppressive role for these cells [32]. This debate reveals the importance of studying MSCs in their unique microenvironment and the pro- or anti-inflammatory signals they may receive in situ. Therefore, we next investigated the role of control MSCs in tumor development. While MSC-mIFNγ suppresses tumor growth and increases overall survival, an equivalent number of control MSCs did not produce any significant effect (pro- or anti-tumor) when compared to PBS treated mice (Fig. 4A). Moreover, mice that received 1×10^5 MSC-mIFNγ, the MED, or a mixture of 1×10^5 MSC-mIFNγ/9 $\times 10^5$ control MSC in a single injection demonstrated a statistically similar outcome (Fig. 4B). These data

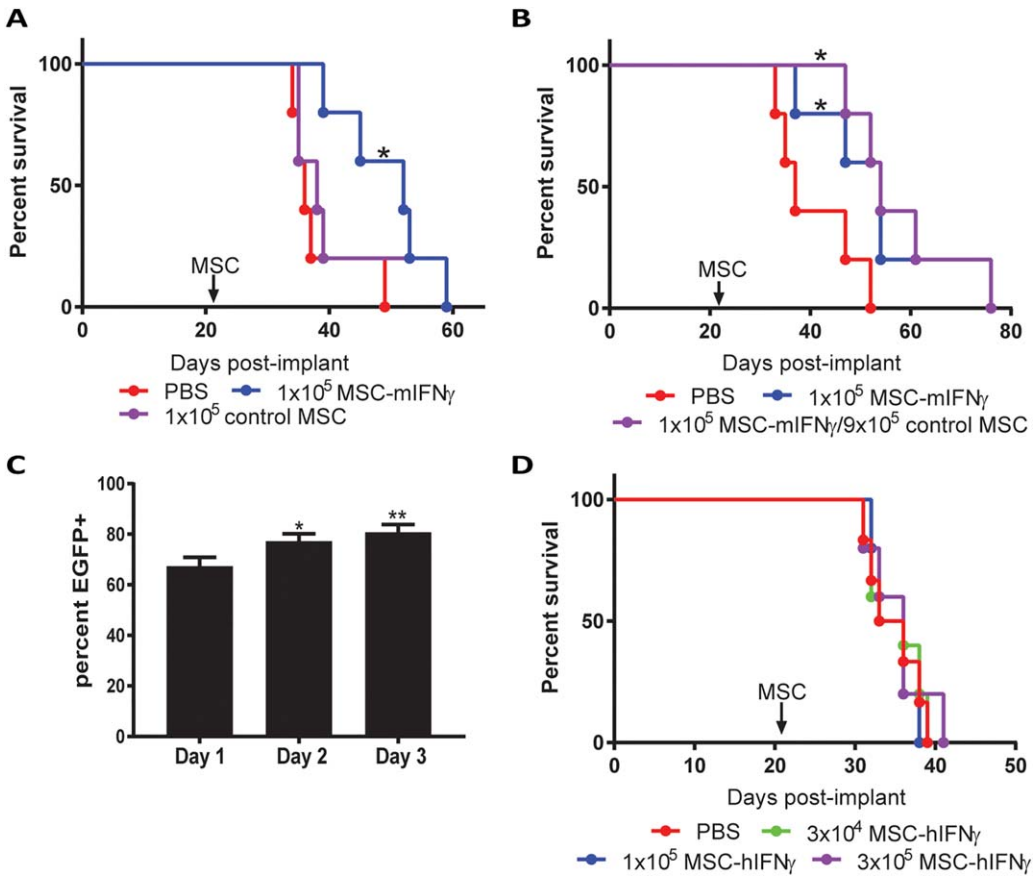

Figure 4. MSCs are not immune suppressive in this model. CHLA-255-luc tumors were treated with PBS ($n = 5$), 1×10^5 MSC-mIFNγ ($n = 5$) or 1×10^5 control MSC ($n = 5$) **(A)**. Control MSCs did not affect survival, while MSC-mIFNγ increased overall survival ($p = .0198$). CHLA-255-luc tumors were treated with PBS ($n = 5$), 1×10^5 MSC-mIFNγ ($n = 5$) or a mixture of 1×10^5 MSC-mIFNγ and 9×10^5 control MSC ($n = 5$) **(B)**. A ninefold excess of control MSCs did not alter survival, while increased overall survival was observed in MSC-mIFNγ ($p = .0466$) and MSC mixture groups ($p = .0180$). Bicistronic lentiviral vector that expresses hIFNγ and EGFP reaches peak infectivity 3 days post-infection in human MSCs (Day 2 $p = 0.0161$, Day 3 $p = 0.0039$) **(C)**. CHLA-255-luc tumors treated with PBS ($n = 6$), 3×10^5 MSC-hIFNγ ($n = 5$), 1×10^5 MSC-hIFNγ ($n = 5$), or 3×10^4 MSC-hIFNγ ($n = 5$) demonstrated no significant difference **(D)**. Abbreviations: EGFP, enhanced green fluorescent protein; hIFNγ, human interferon-gamma; mIFNγ, murine interferon-gamma; MSC, mesenchymal stromal cell; PBS, phosphate buffered saline.

demonstrate that a ninefold excess of unmodified MSCs does not hinder the IFNγ-induced suppression of tumor growth nor the consequent survival.

To identify a direct effect of IFNγ on the tumor cells and/or MSCs (both human origin), we generated a lentiviral vector expressing human IFNγ (hIFNγ) using the same vector backbone. Similar to the mIFNγ vector, MSCs reached peak expression at 3 days post-infection (Fig. 4C). MSC-hIFNγ demonstrated a delayed growth rate when compared to MSC and MSC-mIFNγ, indicating a species-specific response to IFNγ (Supporting Information Fig. S1). Mice treated with tumor injections of MSC-hIFNγ did not show a survival difference compared with controls (Fig. 4D). This finding demonstrates that IFNγ does not have a role in direct tumor cytotoxicity nor in autocrine stimulation of the MSCs toward an immunosuppressive phenotype, thereby promoting tumor proliferation. Additionally, MSC-secreted IFNγ has been reported to stimulate TRAIL secretion from MSCs in an autocrine fashion [33, 34]. Our data suggest that such a mechanism is not a major component in this model, as MSC-hIFNγ injection conveyed neither survival reduction nor benefit.

Role of Macrophages in Tumor

At this juncture, our data suggest MSC-mIFNγ therapy suppresses tumor proliferation without a direct effect on the tumor or MSCs. In our nude mouse xenograft, T cells are lacking but B cells and the entire innate immune system are intact. To begin to elucidate the mechanism of IFNγ activity, we assessed the effect of treating CHLA-255-luc tumors generated in NSG, which do not have any intact innate or adaptive immune function. MSC-mIFNγ treatment did not promote survival in these mice, indicating that monocyte/macrophages, NK cells, or B cells must underlie the survival benefit observed in our nude mouse model (Fig. 5A).

While neither NK cells nor B cells respond to IFNγ, this cytokine is considered one of the most potent pro-inflammatory macrophage activators. Hence, we focused on the role of TAMs, which generally express an immune-suppressive M2 phenotype [35]. Ablating host macrophages via liposomal clodronate removed the therapeutic benefit of MSC-mIFNγ, indicating a macrophage-specific mechanism of effect (Fig. 5B). However, macrophage prevalence within the non-ablated tumors, as defined by CD45+ CD11b+ F4/80+

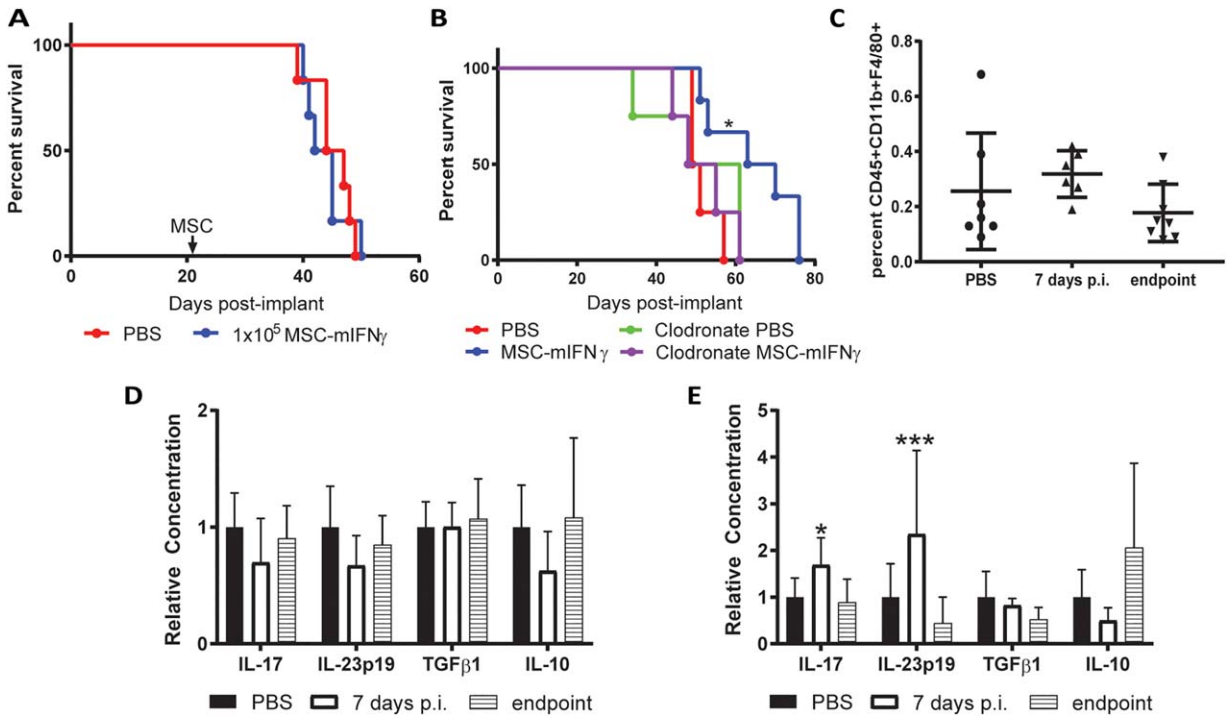

Figure 5. MSC-mIFNγ transiently repolarize macrophages to M1 phenotype. CHLA-255-luc tumor-bearing NSG mice treated with PBS ($n = 6$) or 1×10^5 MSC-mIFNγ ($n = 6$) demonstrated no difference between groups **(A)**. Host macrophages were ablated from CHLA-255-luc tumor-bearing athymic mice via liposomal clodronate or were treated with control liposomes. Tumors were treated with PBS ($n = 5$ control, $n = 4$ clodronate) or 1×10^5 MSC-mIFNγ ($n = 4$) **(B)**. Only control liposome treatment and MSC-mIFNγ increased overall survival ($p = .0226$). MSC-mIFNγ treated tumors from athymic mice were collected at 7 days p.i. and at endpoint; PBS-treated tumors were collected at endpoint only. CD45+ CD11b+ F4/80+ macrophage infiltration did not differ significantly between groups **(C)**. IL-17, IL-23p19, TGFβ1, and IL-10 cytokine expression did not differ in any group of serum collected **(D)**, while the tumor interstitial fluid of MSC-mIFNγ treated tumors revealed increased expression of IL-17 ($p = .0115$) and IL-23p19 ($p = .0010$) at 7 days post-injection **(E)**. Abbreviations: mIFNγ, murine interferon-gamma; MSC, mesenchymal stromal cell; NSG, NOD SCID gamma mice; PBS, phosphate buffered saline; p.i., post injection.

cells, did not differ significantly between PBS treated tumors at endpoint and MSC-mIFNγ treated tumors at 7 days post treatment and at endpoint (Fig. 5C). This observation indicates that MSC-mIFNγ do not increase macrophage infiltration into the tumor.

At point of sacrifice, whole blood was collected via terminal cardiac bleed. Serum was isolated and analyzed alongside TIF. At 7 days post MSC-mIFNγ cell injection or at endpoint, TIF and serum obtained from the animals were assessed in parallel for cytokine content. We did not detect significant differences in serum cytokine expression between these three groups, indicating a tumor-localized effect (Fig. 5D). TIF at 7 days post-MSC-mIFNγ treatment showed significantly elevated levels of two uniquely M1 inflammatory cytokines, IL-17 and IL-23p19 [24–28]. Unique M2 cytokines IL-10 and TGFβ1 were unchanged in the TIF (Fig. 5E). These data support the hypothesis that MSC-mIFNγ transiently repolarize a limited subset of TAMs, possibly those located proximal to the mIFNγ-secreting MSCs. M2 polarized TAMs do not secrete any IL-23p19 or IL-17; hence, small increases in secretion are easily measurable. By contrast, the relative abundance of M2 cytokines renders small reductions undetectable. These data are important because, in contrast to surface marker expression, cytokine release is a functional measure of macrophage polarization.

The serum of treated animals did not show an increase of IFNγ, suggesting that the cytokine does not enter the systemic circulation. This is consistent with the lack of systemic toxicity. Interestingly, however, we did not detect increased IFNγ in the TIF of treated tumors. Given that we detected M1 macrophage derived cytokines, IFNγ must have activated the TAMs. Rapid IFNγ receptor binding/uptake or degradation within the tumor may explain this observation. Nonetheless, our data collectively indicate that MSC-mIFNγ treatment stimulates a transient pro-inflammatory state within the TME, likely conferring the observed tumor suppression.

Discussion

Neuroblastoma persists as a devastating disease despite recent advances in cancer therapeutics [36, 37]. In this work, we used an intra-adrenal xenograft in an effort to most faithfully model the role of the TME in the clinical setting [38]. This model recapitulates the metastatic pattern of neuroblastoma, with identifiable distant metastases in the lungs and liver. We demonstrate that MSCs can be engineered to directly deliver IFNγ to the TME without systemic cytokine exposure, thereby suppressing tumor growth and extending survival in two murine models.

The TME remains one of the largest challenges to successful cancer therapies. Through physical and chemical barriers to therapy penetrance, including a dense extracellular matrix, tortuous vasculature, aberrant metabolism, and immune suppression, tumors are able to evade detection and immune-

mediated killing [4]. Altering the TME to facilitate drug delivery and impact represents a major goal in oncology. Here, we show that MSC-IFNγ promotes an inflammatory microenvironment and boosts the tumor-responsiveness of resident macrophages. Thus, our data represent a significant proof-of-concept that we can effectively retrain a patient's endogenous immune system to recognize and respond to cancer.

Cell delivery of IFNγ has many advantages over traditional systemic infusion. Most importantly, direct injection into the tumor bypasses systemic exposure to IFNγ and the associated toxicities. Additionally, the duration of MSC activity represents a window of continuous IFNγ infusion into the TME as opposed to a single large dose. Finally, multiple studies have shown that intravenously infused MSCs can directly traffic to select tumors, denoting the tumor homing potential of MSCs [39–41]. Therefore, potential applications of this work include systemic infusion of MSC-IFNγ, which then home to the primary tumor as well as distant metastases in order to alter the TME at multiple sites. The possibility of a systemically infused tumor homing therapy represents an intriguing new frontier in the use of MSCs in cancer treatment.

We made extensive use of athymic nude mice as the xenograft hosts; this experimental design bears great significance for the interpretation of our data. In the absence of T cells, eradication of the tumor is not expected. Macrophage activity alone will, at best, impede tumor growth or temporarily lessen the volume of a slowly progressive tumor. Thus, our data demonstrating short-term tumor suppression is clinically significant and suggests this approach holds promise. Additionally, we can conclude that MSCs do not directly promote the tumor and do not counter the IFNγ effect on macrophages in this model.

The next step in development will be to assess the effect of MSC-IFNγ cell therapy in a fully immune competent animal model. To obtain full advantage from this treatment model, repolarized macrophages, and possibly dendritic cells, must present antigens and activate T cells. These effector T cells would then secrete IFNγ and possibly initiate a cytokine feedback loop, obviating the need for ongoing MSC-IFNγ therapy. Moreover, repolarization of TAMs might enhance the therapeutic effects of other immune therapies such as chimeric antigen receptor T (CAR-T) cell therapy. Combining MSC-IFNγ with other approved immunotherapies has the potential to synergistically improve treatment, but determining which combinations are most effective must be empirically determined.

TIF analysis reveals a macrophage-dependent mechanism for the observed survival benefit of MSC-IFNγ. Increased cytokine expression of IL-23p19 and IL-17 within the TIF can only be attributed to resident M1 macrophages, as other potential sources such as T cells are absent in this model. Changes in M1 cytokines were detectable, but a relatively small change of M2 cytokines on a substantial background of TAMs was not statistically detectable. MSC-mIFNγ treatment confers an unambiguous survival benefit in a T cell deficient model, and cytokine analysis reveals a functional repolarization of TAMs to the M1 phenotype. Moreover, the absence of significant survival benefit in NSG mice and macrophage-ablated mice also supports this macrophage-based mechanism.

The observed survival difference between MSC-IFNγ and MSC vehicle-only groups indicates that IFNγ must be produced by the cells, but the absence of increased IFNγ in the TIF suggests that IFNγ is rapidly bound to neighboring cells. Therefore, the effect on macrophage repolarization may be limited locoregionally to the most proximal TAMs. This suggests that a more diffuse injection of MSCs throughout the tumor might increase treatment response, but such a strategy is not feasible within this murine xenograft tumor model. The small tumor size at time of treatment, 0.5–1 volume equivalents of the kidney (~0.2 cm^3) [42], restricts treatment to one injection site so as not to destroy tumor tissue via multiple needle insertions. This limitation would not be relevant to the clinical setting as patients can easily receive injections into multiple regions of the tumor, thereby dispersing the MSCs throughout. Similarly, tumor size limits the total volume and number of MSCs that can be delivered in this model. Future studies will need to evaluate the optimal treatment volume, cell dose, and injection sites for MSC-IFNγ.

A major asset of this treatment strategy is the absence of increased macrophage infiltration into the tumor. This is an important observation, although not unexpected as IFNγ's major effect on macrophages is polarization and classic activation [43, 44]. Because the effect on TAMs is short-term, increased macrophage infiltration into the tumor could ultimately result in greater concentration of tumor-supportive TAMs. This has important implications for clinical translation, as a rebound effect in tumor growth following MSC clearance would potentially negate any conferred treatment benefit.

Conclusion

Our findings establish a proof-of-concept that IFNγ-secreting MSCs can be injected into a solid tumor, impact tumor progression, and confer prolonged survival to the host. While our data implicate repolarization of TAMs, future studies are required to fully elucidate the mechanism of anti-tumor activity. Moreover, macrophage directed therapy in T cell competent host may show remarkably greater activity than in immune deficient models. Our future efforts will build on this essential first step in the development of MSC-IFNγ as a viable treatment strategy in patients.

Acknowledgments

This work was partially supported by the CancerFree Kids Foundation, Families for a Cure Foundation, Ohio State Cancer Center Support Grant, and the Research Institute at Nationwide Children's Hospital. E.M.H. is currently affiliated with Aflac Cancer and Blood Disorders Center, Children's Healthcare of Atlanta, Emory University Department of Pediatrics, Atlanta, GA.

Author Contributions

T.R.: conception and design, collection and/or assembly of data, data analysis and interpretation, manuscript writing, final approval of manuscript; A.J.G.: conception and design, provision of study material, data analysis and interpretation; K.L.P.: collection and/or assembly of data, data analysis and interpretation; S.O.: conception and design, data analysis and interpretation; T.Y. and S.H.: collection and/or assembly of data; M.D.: final approval of manuscript; C.B.: financial support; E.M.H.: conception and design, financial support, provision of study material, data analysis and interpretation, final approval of manuscript.

Disclosure of Potential Conflicts of Interest

M.D. discloses Advisory role and stock ownership in Rigenerand srl. C.B. discloses intellectual and ownership interest in LYST Therapeutics, Pall Corporation and research funding from Gunze Limited. E.M.H. discloses honorarium from Current Stem Cell Reports (journal) for service as Section Editor and stock ownership in Pluristem Therapeutics, Inc. The other authors indicated no potential conflicts of interest.

References

1 Brodeur GM. Neuroblastoma: Biological insights into a clinical enigma. Nat Rev Cancer 2003;3:203–216.
2 Maris JM. Recent advances in neuroblastoma. N Engl J Med 2010;362:2202–2211.
3 Yang RK, Sondel PM. Anti-gd2 strategy in the treatment of neuroblastoma. Drugs Future 2010;35:665.
4 Relation T, Dominici M, Horwitz EM. Concise review: An (im)penetrable shield: How the tumor microenvironment protects cancer stem cells. Stem Cells 2017;35:1123–1130.
5 Blonska M, Agarwal NK, Vega F. Shaping of the tumor microenvironment: Stromal cells and vessels. Semin Cancer Biol 2015;34:3–13.
6 Whiteside TL. The tumor microenvironment and its role in promoting tumor growth. Oncogene 2008;27:5904–5912.
7 D'Souza N, Rossignoli F, Golinelli G et al. Mesenchymal stem/stromal cells as a delivery platform in cell and gene therapies. BMC Med 2015;13:186.
8 Grisendi G, Bussolari R, Veronesi E et al. Understanding tumor-stroma interplays for targeted therapies by armed mesenchymal stromal progenitors: The Mesenkillers. Am J Cancer Res 2011;1:787–805.
9 Horwitz EM, Gordon PL, Koo WK et al. Isolated allogeneic bone marrow-derived mesenchymal cells engraft and stimulate growth in children with osteogenesis imperfecta: Implications for cell therapy of bone. Proc Natl Acad Sci USA 2002;99:8932–8937.
10 Hui L, Chen Y. Tumor microenvironment: Sanctuary of the devil. Cancer Lett 2015;368:7–13.
11 Dunn GP, Koebel CM, Schreiber RD. Interferons, immunity and cancer immunoediting. Nat Rev Immunol 2006;6:836–848.
12 Miller CH, Maher SG, Young HA. Clinical use of interferon-gamma. Ann NY Acad Sci 2009;1182:69–79.
13 Parker BS, Rautela J, Hertzog PJ. Antitumour actions of interferons: Implications for cancer therapy. Nat Rev Cancer 2016;16:131–144.
14 Welm BE, Dijkgraaf GJ, Bledau AS et al. Lentiviral transduction of mammary stem cells for analysis of gene function during development and cancer. Cell Stem Cell 2008;2:90–102.
15 Otsuru S, Hofmann TJ, Olson TS et al. Improved isolation and expansion of bone marrow mesenchymal stromal cells using a novel marrow filter device. Cytotherapy 2013;15:146–153.
16 Dominici M, Le Blanc K, Mueller I et al. Minimal criteria for defining multipotent mesenchymal stromal cells. The international society for cellular therapy position statement. Cytotherapy 2006;8:315–317.
17 Englen MD, Valdez YE, Lehnert NM et al. Granulocyte/macrophage colony-stimulating factor is expressed and secreted in cultures of murine L929 cells. J Immunol Methods 1995;184:281–283.
18 Guess AJ, Daneault B, Wang R et al. Safety profile of good manufacturing practice manufactured interferon gamma-primed mesenchymal stem/stromal cells for clinical trials. Stem Cells Translational Medicine 2017;6:1868–1879.
19 Haslene-Hox H, Oveland E, Berg KC et al. A new method for isolation of interstitial fluid from human solid tumors applied to proteomic analysis of ovarian carcinoma tissue. PLoS One 2011;6:e19217.
20 Song L, Ara T, Wu HW et al. Oncogene MYCN regulates localization of NKT cells to the site of disease in neuroblastoma. J Clin Invest 2007;117:2702–2712.
21 Shimada H, Ambros IM, Dehner LP et al. Terminology and morphologic criteria of neuroblastic tumors: Recommendations by the international neuroblastoma pathology committee. Cancer 1999;86:349–363.
22 Dubois SG, London WB, Zhang Y et al. Lung metastases in neuroblastoma at initial diagnosis: A report from the international neuroblastoma risk group (inrg) project. Pediatr Blood Cancer 2008;51:589–592.
23 Jablonski KA, Amici SA, Webb LM et al. Novel markers to delineate murine m1 and m2 macrophages. PLoS One 2015;10:e0145342.
24 Arnold CE, Whyte CS, Gordon P et al. A critical role for suppressor of cytokine signalling 3 in promoting m1 macrophage activation and function in vitro and in vivo. Immunology 2014;141:96–110.
25 Carson WF 4th, Salter-Green SE, Scola MM et al. Enhancement of macrophage inflammatory responses by CCL2 is correlated with increased miR-9 expression and downregulation of the ERK1/2 phosphatase Dusp6. Cell Immunol 2017;314:63–72.
26 Van den Bossche J, Baardman J, Otto NA et al. Mitochondrial dysfunction prevents repolarization of inflammatory macrophages. Cell Rep 2016;17:684–696.
27 Sica A, Mantovani A. Macrophage plasticity and polarization: In vivo veritas. J Clin Invest 2012;122:787–795.
28 Geng Y, Zhang L, Fu B et al. Mesenchymal stem cells ameliorate rhabdomyolysis-induced acute kidney injury via the activation of M2 macrophages. Stem Cell Res Ther 2014;5:80.
29 Bernardo ME, Fibbe WE. Mesenchymal stromal cells: Sensors and switchers of inflammation. Cell Stem Cell 2013;13:392–402.
30 Metelitsa LS, Wu HW, Wang H et al. Natural killer T cells infiltrate neuroblastomas expressing the chemokine CCL2. J Exp Med 2004;199:1213–1221.
31 Fischer UM, Harting MT, Jimenez F et al. Pulmonary passage is a major obstacle for intravenous stem cell delivery: The pulmonary first-pass effect. Stem Cells Dev 2009;18:683–692.
32 De Miguel MP, Fuentes-Julian S, Blazquez-Martinez A et al. Immunosuppressive properties of mesenchymal stem cells: Advances and applications. Curr Mol Med 2012;12:574–591.
33 Yang X, Du J, Xu X et al. IFN-γ-secreting-mesenchymal stem cells exert an antitumor effect in vivo via the trail pathway. J Immunol Res 2014;2014:1.
34 Du J, Zhou L, Chen X et al. IFN-γ-primed human bone marrow mesenchymal stem cells induce tumor cell apoptosis in vitro via tumor necrosis factor-related apoptosis-inducing ligand. Int J Biochem Cell Biol 2012;44:1305–1314.
35 Noy R, Pollard JW. Tumor-associated macrophages: From mechanisms to therapy. Immunity 2014;41:49–61.
36 Speleman F, Park JR, Henderson TO. Neuroblastoma: A tough nut to crack. Am Soc Clin Oncol Educ Book 2016;35:e548–e557.
37 Esposito MR, Aveic S, Seydel A et al. Neuroblastoma treatment in the post-genomic era. J Biomed Sci 2017;24:14.
38 Braekeveldt N, Wigerup C, Tadeo I et al. Neuroblastoma patient-derived orthotopic xenografts reflect the microenvironmental hallmarks of aggressive patient tumours. Cancer Lett 2016;375:384–389.
39 Reagan MR, Kaplan DL. Concise review: Mesenchymal stem cell tumor-homing: Detection methods in disease model systems. Stem Cells 2011;29:920–927.
40 Sun Z, Wang S, Zhao RC. The roles of mesenchymal stem cells in tumor inflammatory microenvironment. J Hematol Oncol 2014;7:14.
41 Yagi H, Kitagawa Y. The role of mesenchymal stem cells in cancer development. Front Genet 2013;4:261.
42 Wallace DP, Hou YP, Huang ZL et al. Tracking kidney volume in mice with polycystic kidney disease by magnetic resonance imaging. Kidney Int 2008;73:778–781.
43 Frucht DM, Fukao T, Bogdan C et al. IFN-γ production by antigen-presenting cells: Mechanisms emerge. Trends Immunol 2001;22:556–560.
44 Schoenborn JR, Wilson CB. Regulation of interferon-gamma during innate and adaptive immune responses. Adv Immunol 2007;96:41–101

See www.StemCells.com for supporting information available online.